The 2012 World Congress on
Advances in Civil, Environmental, and Materials Research (ACEM' 12)
Seoul, Korea, August 26-30, 2012

Examining K_0 and Stiffness Changes in Sand under Different Loading Conditions

*Yan GAO[1)] and Yu-Hsing, WANG[2)]

[1), 2)] *Department of Civil and Environmental Engineering, The Hong Kong University of Science and Technology, Hong Kong, P.R. China*
[1)] gylyq@ust.hk

ABSTRACT

This paper examines how and why K_0 and the small-strain shear modulus of sand (Dry Leighton Buzzard sand) changes in response to different loading conditions. The experiment was carried out using a modified oedometer equipped with a bender element system and the tactile pressure sensor. The tactile sensors were used to measure the horizontal stress σ_h and the vertical stress σ_v. The two shear moduli, i.e., G_{hh} and G_{hv}, were continuously monitored using the bender element system. It is found in the experiment that G_{hv} is greater than G_{hh} under the K_0-stress condition. Both of G_{hv} and G_{hh} continuously increase with time during the process of structuration taking place at secondary compression. The modulus change is also larger in G_{hv} than in G_{hh}. The K_0 value is kept constant during loading but continues to increase during secondary compression. The corresponding numerical simulations via the discrete element method (DEM) were also carried out and reproduced these experimental findings. During the structuration process taking place at secondary compression, contact creep makes the contact forces among soil particles become more homogeneous, which in turns strengthen the soil. In addition, greater creep taking place in the vertical direction than in the horizontal direction; this explains a greater change in G_{hv} than in G_{hh}.

1. INTRODUCTION

K_0-stress condition is one of the important stress states in engineering design. In general, Jaky's equation (Jaky 1944), 1-sin′ϕ where ϕ' is the friction angle, is used to simple estimate K_0. Published results have clearly shown K_0 of sand is constant to elevated pressures during loading and increases with increasing overconsolidation ratio, OCR, during unloading (e.g., Ghionna et al. 1981; Feda 1984; Yamamuro et al. 1996). Yamamuro et al. (1996) demonstrated that K_0 continues to increase during secondary compression; however, the applied pressure, 839 MPa, was high and particle crushing might occur. When the applied pressure is not high to make particle crushed, the

[1)] Graduate Student
[2)] Professor

associated K_0 responses during secondary compression however are not known yet. Hence, the first objective of this paper is to resolve this unknown. The structuration or aging process takes place during secondary compression (e.g., Schmertman 1991, Lagioia 1998, Lade et al. 2009). Hence, another objective of this study is to monitor the structuration process using the wave-based techniques, i.e., monitoring the associated stiffness changes. The numerical simulations by the discrete element method (DEM) are also carried out to provide explanations from the micromechanical perspective.

2. EXPERIMENTAL DETAILS

A modified oedometer apparatus, as shown in Fig. 1, was used to investigate the stiffness changes during the process of structuration. The tailor-made oedometer cell with an inner dimension of 100 mm × 100 mm × 40 mm was equipped with a bender element system and the tactile pressure sensors. The Leighton Buzzard sand (fraction E) with a relative round particle shape was tested. Therefore, the inherent fabric-induced anisotropy can be ignored. Its grain size distribution is between 0.425 mm and 0.063 mm. A dense sand sample with a density of ~1.6 g/cm^3 was prepared. During the test, the vertical stress σ_v was gradually increased from 0 to 50 kPa with an increment of 10 kPa. Then, the stress was kept constant at 50 kPa for three days of secondary compression for developing the structuration process.

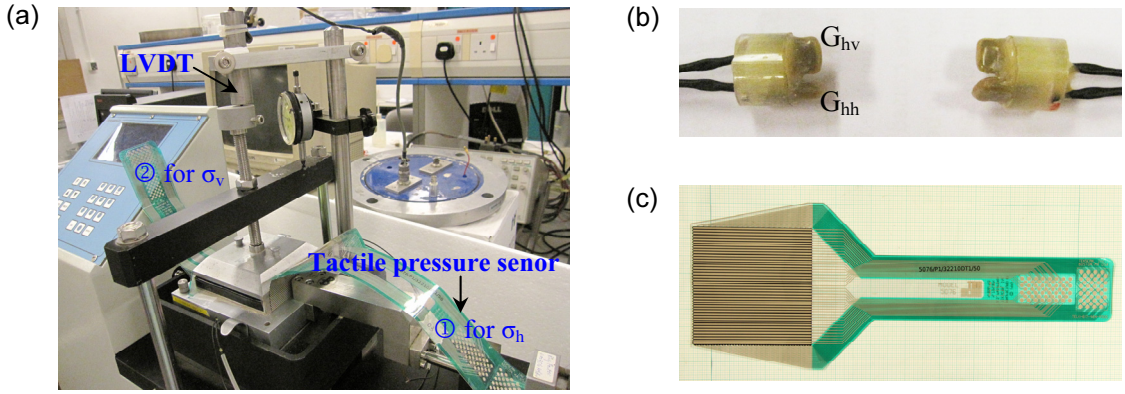

Fig. 1 Experimental setup and sensors installed: (a) the setup, (b) bender element system, and (c) tactile pressure sensor.

A bender element system as shown in Fig. 1b was embedded inside the sample to continually monitor the stiffness change in the experiment. Four bender elements in two sets were included in the system. In each set, there were one bender element as source and the other one as the receiver. The tip-to-tip distance *d* between the source and the receiver was set to be 80 mm and kept constant during the test. The associated travel time *t* was determined through the first peaks of the source and receiver signals. Then, the shear wave velocity V_s and the corresponding small-strain shear modulus G can be computed by $G = \rho V_s^2 = \rho(d/t)^2$ where ρ is the sample density.

Two shear moduli G_{hh} and G_{hv} can be obtained where the first and the second subscripts represent the directions of wave propagation and polarization, respectively. The symbols, h and v stand for the horizontal and vertical directions, respectively. The tactile pressure sensors (illustrated in Figs. 1 and 1c) was used to measure the horizontal stress σ_h and vertical stress σ_v.

3. EXPERIMENTAL RESULTS

Fig. 2 presents the experimental results of the shear modulus. When the vertical stress is increased from 10 kPa to 50 kPa, G_{hv} increases from ~42 kPa to ~102 kPa while G_{hh} rises from ~34 kPa to ~85 kPa. In addition, Ghv is always greater than Ghh. This is due to a higher stress in the vertical direction than in the horizontal direction, and the shear modulus depends on the in-plane stresses (Roesler 1979, Stokoe et al., 1985, 1991, and 1995; Wang and Mok 2008). During three days secondary compression, the structuration develops and the shear moduli increase because the sample becomes stronger. The associated changes are shown in Fig. 2b where the modulus change is defined as $(G_t-G_{in})/G_{in}$ to quantify the shear modulus variations with time. The G_t and G_{in} are the shear moduli at any time t and at the initial state, respectively. It can be readily seen that the stiffness change is also higher associated with G_{hv} than associated with G_{hh}. Fig. 3 gives the void ratio variations during the test. The void ratio decreases from 0.7272 to 0.7063 when the vertical stress increases from 10 kPa to 50 kPa. The percentage change is ~2.9%. During the three days secondary compression at σ_v = 50 kPa, the void ratio continues to decrease by ~0.3%. At the same time as shown in Fig. 2b, the shear moduli increase by ~2.8% and ~2.0% for G_{hv} and G_{hh}, respectively. The underlying mechanisms for such a modulus change are further discussed later based on DEM simulations.

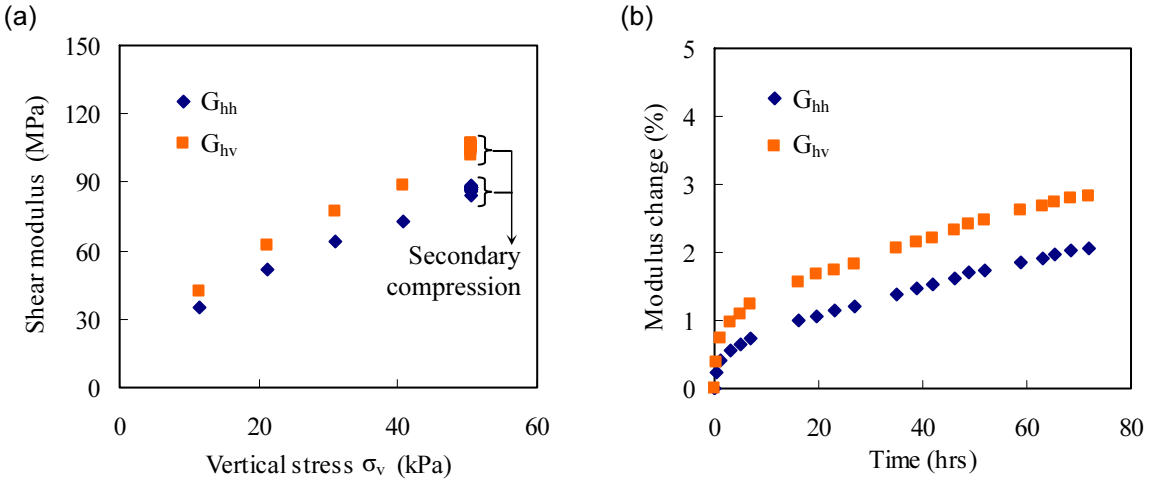

Fig. 2 Experimental results: (a) shear moduli versus the applied vertical stress σ_v, and (b) changes of the shear moduli with time during secondary compression at σ_v = 50 kPa.

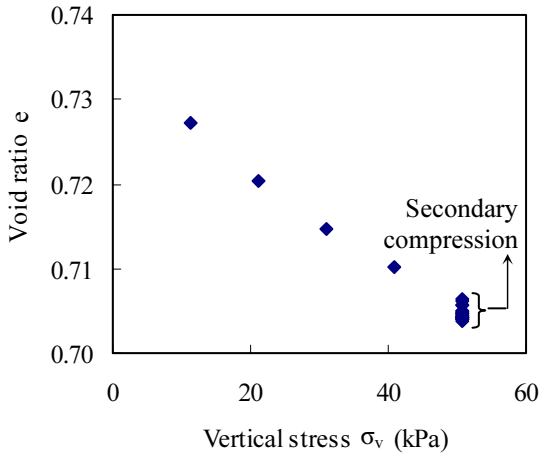

Fig. 3 Void ratio versus vertical stress σ_v.

The stresses measured by the tactile pressure sensors are exhibited in Fig. 4. It is easy to see that when the vertical stress (σ_v, measured by sensor②) increases, the horizontal stress (σ_h, measured by sensor①) increases as well. The ratio of σ_h to σ_v (i.e., the K_0 value) is kept constant around 0.53 during the loading stage as shown in Fig. 4b. During the structuration process taking place at secondary compression, σ_h increases while σ_v is not changed and an increase in K_0 is obtained. After three days, K_0 is increased to ~0.56 and the increment is ~6.8%.

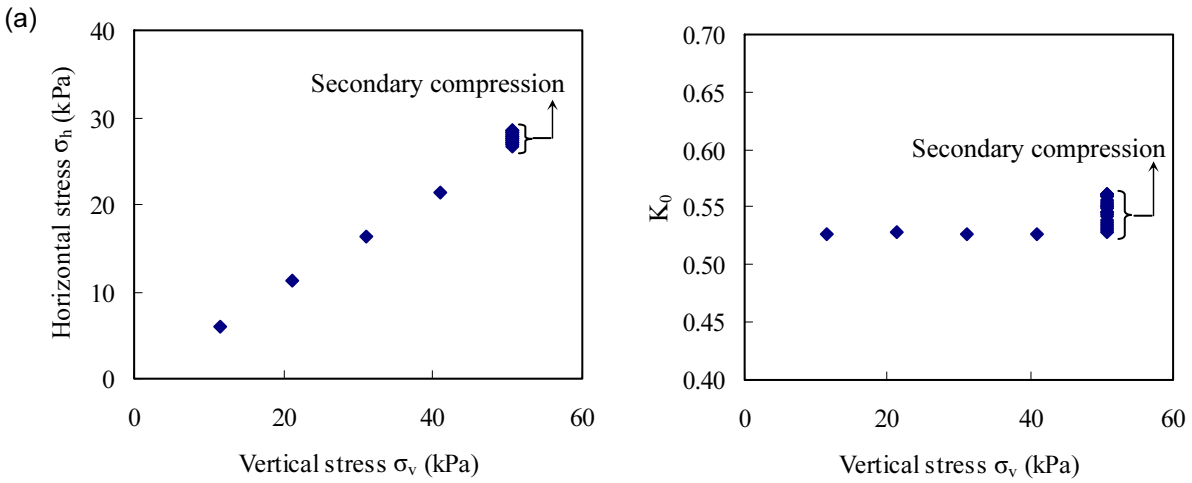

Fig. 4 K_0 evolutions with the applied vertical stress based on experimental results: (a) horizontal stress versus vertical stress, and (b) K_0 variations.

4. DEM SIMULATIONS AND RESULTS

The PFC 3D (Itasca Consulting Group, Minn.) based on the discrete element method was used to simulate the experimental findings. The sample packing is shown in Fig. 5; there are 15208 balls randomly generated in a box with a dimension of 100

mm × 100 mm × 40 mm. The box was composed of six rigid walls, which are used to apply loading. Table 1 summarizes the parameters used in the simulations. During the loading stage, the Hertz-Mindlin contact model was used to simulate the stress-dependent soil properties. During the structuration process at constant stress of 50, the viscous contact model was adopted to capture the time dependent behavior, i.e., the Burgers' model. At different stress states, a shearing test was conducted to get the shear modulus. Note that, the shear strain was controlled in 10^{-6} for a small-strain condition. Details of the contact models used in the DEM simulations can be referred to Gao et al. (2012).

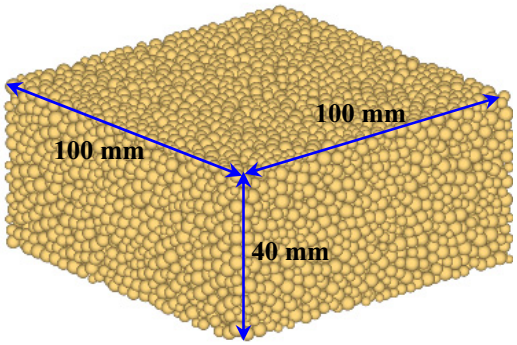

Fig. 5 The numerical sample used in the DEM simulations.

Table 1 Parameters adopted in DEM simulations.

Model Parameters		Adopted values	
Soil particle properties			
Particle density		2650	(kg/m^3)
Particle diameter		0.1-0.2	(mm)
Number of particles		15028	
Friction coefficient		0.2	
Contact Model (Hertz-Mindlin model)	Shear modulus, G	5	(GPa)
	Poisson's ratio, ν	0.2	
Model for creep (Burger's model)			
	Dashpot of the Maxwell unit, C_1	10^7	(N·s/m)
	Dashpot of the Kelvin unit, C_2	10^6	(N·s/m)
	Spring constants, k^s_1 and k^s_2	Based on the Hertz-Mindlin model	
Rolling resistance	J_n	0.5	
	η	0.5	
Wall properties			
Normal contact stiffness		10^8	(N)
Friction coefficient	During loading	0.0	

Figs. 6 and 7 present the modulus and K_0 variations obtained from the DEM simulations. The void ratio change during the secondary compression is controlled at 0.3%, which is similar to the experimental results. The simulation results reproduce the experimental results. G_{hv} is larger than G_{hh} and the associated change with time is also higher than that for G_{hh}. The K_0 is constant during the loading stage and increases with time during the secondary compression.

5 MICROMECHANICAL EXPLANATIONS

To investigate the underlying mechanism, the micromechanical properties of the samples at different loading states are examined. As illustrated in Fig. 7, Point A (at σ_v = 20 kPa) is selected as the initial state. Points B and C are the states before and after secondary compression at σ_v = 50 kPa (i.e., during structuration process). The mean, standard deviation (SD), coefficient of variance (CV) and the percentage of weak forces (POW) for the contact normal forces at horizontal (x) direction F_x and at the vertical (z) direction F_z are summarized in Table 2. The characterization of strong and weak forces (i.e., the contact normal forces at strong and weak contacts or at strong and weak networks) follows the suggestion of Radjai et al. (1996). The normal contact force, F_n, which is greater than its mean, $\langle F_n \rangle$, is regarded as a "strong" force (i.e., $F_n / \langle F_n \rangle > 1$); otherwise it is a "weak" force if $F_n / \langle F_n \rangle < 1$. The percentage of weak forces (POW) means how many percentages of the contact normal forces belong to the weak ones

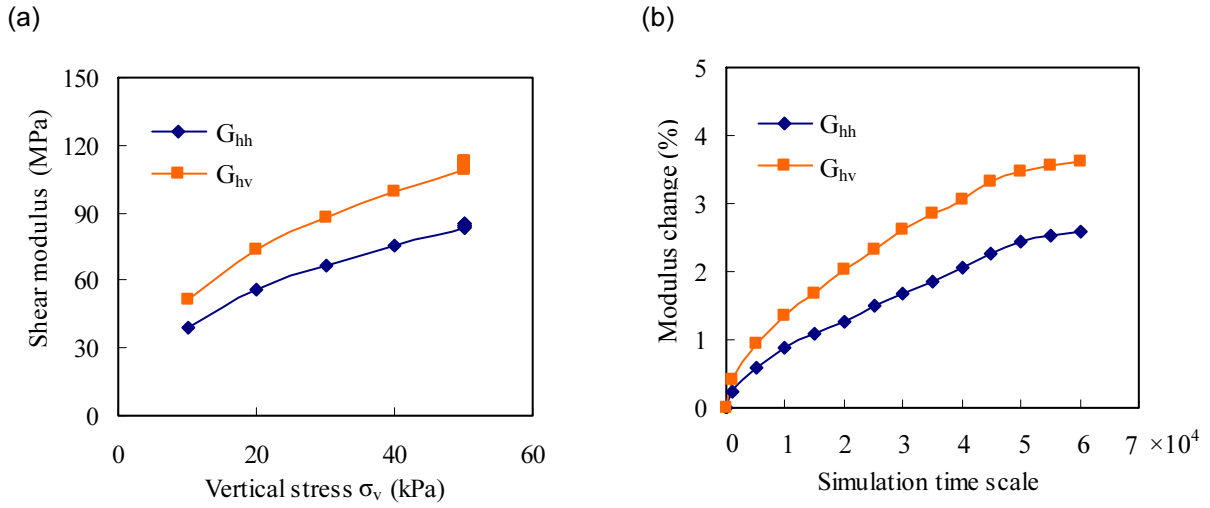

Fig. 6 Simulation results: (a) shear moduli variations versus the applied vertical stress, (b) modulus changes during secondary compression at σ_v = 50 kPa.

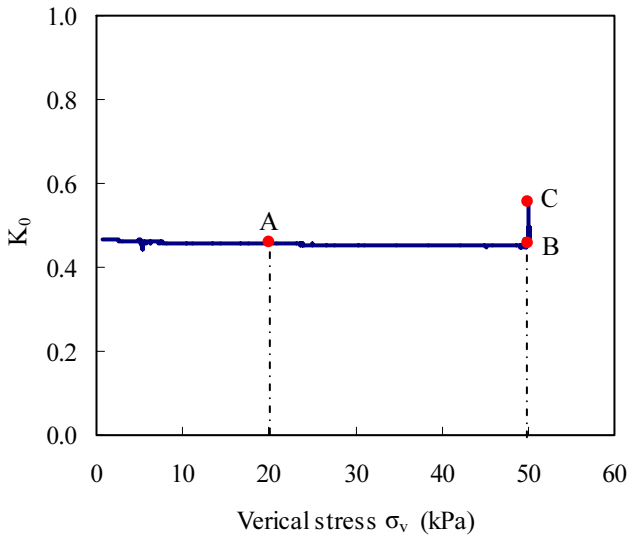

Fig. 7 K_0 evolutions with the applied vertical stress from DEM simulations.

Table 2 Micromechanical properties of soil at points A, B and C in Fig. 7.

	Point A (Initial state)		**Point B (After loading)**		**Point C (After secondary compression)**	
	F_x	F_z	F_x	F_z	F_x	F_z
Mean (N)	706.35	990.74	1716.11	2379.37	1922.53	2584.76
SD (N)	661.04	1228.66	1612.78	2936.89	1816.18	3125.31
CV (N)	0.9359	1.2401	0.9398	1.2343	0.9447	1.2091
POW (%)	61.03	66.47	60.89	66.41	56.88	63.61

During the loading stage if compared with the forces at points A and B, no matter for F_x or F_z, the CV and POW are similar. This similarity suggests that the internal structure and the force transmission are not changed too much during the loading stage. Therefore, a constant K_0 is obtained. During the structuration process taking place at secondary compression, the vertical displacement continues to develop while the horizontal deformation is constrained. Therefore, the horizontal stress increases and so does K_0. Guided by the findings in Gao et al. (2012), we have known that during aging contact forces among particles becomes more homogenized, which is initiated by contact creep. This homogenization process in turn gives rise to a decrease in the percentage of weak forces and an increase in the shear modulus. This finding can also be applied to explain the soil behavior during structuration at secondary compression under a K_0-stress condition. If compared the micromechanical properties at points B and C, it can be found that CV is changed, especially in F_z (decreased by ~2%). The decreasing CV means that the forces become more homogenized after three days of

secondary compression. The percentages of weak forces in F_z and F_x both are decreased. This leads to strengthen the soil and an increase in the associated shear modulus as shown in Fig. 6b. The contact creep is easier to occur in the z direction because the major principal stress is in the z direction and the sample is only allowed to deform in the z direction. Hence, a larger stiffness change is found associated with G_{hv} than associated with G_{hh}.

5. CONCLUSION

The stiffness and K_0 variations under different loading conditions, especially during secondary compression, are studied in this paper using experiments and DEM simulations. The salient findings are summarized as follows:
During the loading stage, G_{hv} is greater than G_{hh} because the stress is higher in the vertical direction than in the horizontal direction. The K_0 value is kept constant as the vertical stress increases. During the structuration process taking place at secondary compression, K_0 continues to increase because of the vertical deformation by creep. The shear modulus also increases with elapsed time. This is due to that contact creep makes the contact forces among soil particles become more homogeneous, which in turns strengthen the soil. The modulus change is also higher associated with G_{hv} than associated with G_{hh}. This can be attributed to greater creep taking place in the vertical direction than in the horizontal direction.

ACKNOWLEDGEMENTS

This research was supported by the Hong Kong Research Grants Council (GRF 620310).

REFERENCES

Alpan, I. (1967), “The empirical evaluation of the coefficient K_0 and K_{0R},” *Soil and Foundation*, Vol.**VII**(1), 31-40.
Gao, Y., Yeung, C.K. and Wang, Y.H. (2012), “Mechanisms of aging-induced modulus Changes in sand under isotropic and anisotropic loading,” *J. Geotech. Geoenviron. Eng.* (daft accepted).
Jaky, J. (1944), “The coefficient of earth pressure at rest,” *J. for Society of Hungarian Architects and Engineers*, Vol. **78**(22), 355-358 (in Hungarian).
Jaroslav Feda (1984), “K_0-coefficient of sand in triaxial apparatus,” *Journal of Geotechnical Engineering*, Vol. **110**(4), 519-524.
Lade, P.V., Liggio, Jr., C.D. and Nam, J. (2009). “Strain rate, creep, and stress drop-creep experiments on crushed coral sand.” *J. Geotech. Geoenviron. Eng.*, ASCE, Vol. **135**(7), 941-953.
Lagioia, R. (1998). ‘‘Creep and apparent preconsolidation in carbonate soils.’’ The geotechnics of hard soil-Soft rocks, A. Evangelista and L. Picarelli, eds., Balkema, Rotterdam, The Netherlands.
Mesri, G. and Hayat, T.M. (1993), “The coefficient of earth pressure at rest,” *Can. Geotech. J.*, Vol. **30**, 647-666.

Mesri, G. and Vardhanabhuti, B. (2007), “Coefficient of earth pressure at rest for sands subjected to vibration,” *Can. Geotech. J.*, Vol. **44**, 1242-1263.
Mesri, G. and Vardhanabhuti, B. (2009), “Compression of granular materials,” *Can. Geotech. J.*, Vol. **46**, 369-392.
Mesri, G., Feng, T.W. and Benak, J.M.(1990), “POSTDENSIFICATION PENETRATION RESISTANCE OF CLEAN SANDS,” *Journal of Geotechnical Engineering*, Vol. **116**(7), 1095-1115.
Mitchell and Soga (2005). Fundamental of soil behavior. 3rd edition, John Wiley & Sons, Inc., New York.
Pan, Y.W. and Liou, J.C. (2004), “K_0 estimation in level granular soil from anisotropic wave velocities on the basis of micromechanics,” *Int. J. of Num. and Ana. Methods in Geomechanics*, Vol. **28**, 1401-1425.
Radjai, F., Jean, M., Moreau, J. J. and Roux, S. (1996). “Force distributions in dense two-dimensional granular systems.” *Phys. Rev. Lett.*, Vol. **77**(2), 274-277.
Roesler, S.K. (1979), “Anisotropic shear modulus due to stress anisotropy,” *Journal of the Geotechnical Engineering Division*, Vol. **7**, 871-880.
Schmertmann, J. H. (1991). “The mechanical aging of soils.” *J. Geotech. Engrg.*, ASCE, Vol. **117**(9), 1286-1330.
Stokoe, K. H. II, Hwang, S. K., Lee, J. N. K. and Andrus, R. D. (1995). “Effects of various parameters on the stiffness and damping of soils at small to medium strains.” Pre-failure deformation of geomaterials : proceedings of the International Symposium on Pre-Failure Deformation Characteristics of Geomaterials, Sapporo, Japan 12-14, September 1994, 785-816.
Stokoe, K. H. II, Lee, J. N. K. and Lee, S. H. H. (1991). “Characterization of soil in calibration chambers with seismic waves.” Calibration chamber testing: proceedings of the first International Symposium on Calibration Chamber Testing/ISOCCT1, Potsdam, New York, 28-29 June 1991, 363-376.
Stokoe, K. H., Lee, S. H. H. and Knox, D. P. (1985). “Shear moduli measurements under true triaxial stresses,” Advances in the Art of Testing Soils Under Cyclic Conditions: proceedings of a session / sponsored by the Geotechnical 182 Engineering Division in conjunction with the ASCE Convention in Detroit, Michigan, ASCE, 166-185
Wang Y.H., Mok, C.M.B. (2008). “Mechanisms of small-strain shear-modulus anisotropy in sands,” *J. Geotech. Geoenviron. Eng.*, ASCE, Vol. **134**(10), 1516-1530.
Yamamuro, J.A., Bopp, P.A. and Lade, P.V. (1996), “One-dimensional compression of sands at high pressure,” *Journal of Geotechnical Engineering*, Vol. **122**(2), 147-154.